



Isolation of bacterial extracellular vesicles from raw samples using a portable microstructured electrochemical device

Valeria Mantella¹ · Siiri Bienz² · Finn Brigger¹ · Edouard Baulier³ · Marie Ramus³ · Nicole Zoratto¹ · Steffen Honrath¹ · Kumar Naresh² · Sibilla Sander⁴ · Jörn Dengjel⁴ · Renato Zenobi² · Vadim Krivitsky⁵ · Jean-Christophe Leroux¹

Received: 2 April 2025 / Accepted: 3 August 2025 / Published online: 26 August 2025
© The Author(s) 2025

Abstract

Bacterial extracellular vesicles (EVs) are nanosized vesicles released by both Gram-negative and Gram-positive bacteria, playing critical roles in microbial communication, host-pathogen interactions, and immune modulation. Despite their significance in research and clinical applications, conventional isolation methods, such as ultracentrifugation (UC), are often slow, labor-intensive, and susceptible to contamination. In this study, we evaluated a novel portable microstructured electrochemical device (PMED) designed for rapid and selective bacterial EV isolation directly from biological samples. Using immunoaffinity-based capture and voltage-triggered release, the device-isolated EVs from Gram-negative *Escherichia coli* (*E. coli*), Gram-positive *Lactobacillus fermentum* (*Lb. fermentum*) culture supernatants and from urine samples spiked with *E. coli*, showing superior purity compared to UC. Characterization through nanoparticle tracking analysis (NTA), dynamic light scattering (DLS), and Western blot confirms enhanced selectivity and reduced contaminants. Functional assays demonstrated that device-isolated *Lb. fermentum* EVs selectively activated Toll-like receptor 4 (TLR4) without triggering TLR2, unlike UC-isolated EVs, suggesting a more refined immunomodulatory effect. These findings highlight the device's translational potential for EV-based diagnostics, particularly for noninvasive urinary tract infection detection, and its broader applications in studying bacterial communication and immune regulation.

Keywords Extracellular vesicles · Bacteria · Electrochemical device · Ultracentrifuge · Immune selectivity

Introduction

Bacterial extracellular vesicles (EVs) are small, membrane-bound vesicles with diameters ranging from 20 to 250 nm [1, 2]. They are released by both Gram-negative (e.g. *Escherichia coli*, *E. coli*) and Gram-positive (e.g. *Lactobacilli*, *Lb.*) bacteria, through different mechanisms that vary according to the structural characteristics of the originating cell [1–3]. In the case of Gram-negative bacteria, EVs (also known as outer membrane vesicles, OMVs) primarily arise from the blebbing of the outer membrane [1–4]. This process is caused by several factors, including an imbalance in peptidoglycan biosynthesis, the intercalation of hydrophobic molecules, or explosive cell lysis induced by phage-derived endolysins that degrade the peptidoglycan cell wall [3, 4]. Given the thicker peptidoglycan layer in Gram-positive bacteria, it was initially believed that they could not release EVs [5]. However, recent research has elucidated that Gram-positive bacteria indeed produce EVs through budding from the cytoplasmic membrane [5].

✉ Vadim Krivitsky
vadimkrivitsky@acytronix.ch

✉ Jean-Christophe Leroux
jleroux@ethz.ch

¹ Laboratory of Drug Formulation and Delivery, Institute of Pharmaceutical Sciences, Department of Chemistry and Applied Biosciences, ETH Zürich, Zürich 8093, Switzerland

² Laboratory of Organic Chemistry, Institute of Pharmaceutical Sciences, Department of Chemistry and Applied Biosciences, ETH Zürich, Zürich 8093, Switzerland

³ OM Pharma SA, Meyrin 1217, Geneva, Switzerland

⁴ Department of Biology, University of Fribourg, Chemin du Musée 10, Fribourg 1700, Switzerland

⁵ Acytronix GmbH, Wagistrasse 18, Schlieren 8952, Switzerland

Overall, bacterial EVs are able to enter host cells and deliver various biomolecules, including proteins, virulence factors, peptidoglycan, and nucleic acids [1, 2, 4–6].

Bacterial EVs can activate both the innate and adaptive immune systems, influencing a variety of biological functions including virulence, horizontal gene transfer, phage infection and transport of bacterial metabolites [1–7]. In host-microbe interactions, EVs contribute to immune modulation, epithelial cell adhesion, and the delivery of bacterial effectors that can influence host cell signaling and pathogen defense mechanisms [8, 9]. In particular, these EVs carry specific molecules known as pathogen-associated molecular patterns (PAMPs) which act as recognizable signals to the host immune system. Common PAMPs include lipoteichoic acid (LTA), lipopolysaccharides (LPS), lipopeptides, peptidoglycan, flagellin, and bacterial DNA [8, 10, 11]. Such molecules are recognized by highly conserved pattern recognition receptors, such as Toll-like receptors (TLRs). For instance, EVs derived from *Lactobacilli* have been shown to boost certain immune responses mediated by TLR2/1 and TLR4 receptors while dampening responses through TLR2/6 [10, 12].

Beyond their immunomodulatory roles, bacterial EVs have emerged as promising biomarkers for liquid biopsy applications, particularly for diagnosing conditions affecting the kidneys, bladder, and urogenital tract, including the prostate, uterus, and vagina [13–17]. While some pathogenic bacteria release EVs that contribute to infection and inflammation, these vesicles also serve as indicators of bacterial presence and activity within specific tissues [11].

Despite increasing interest in bacterial EVs and their diverse roles, their practical implementation remains constrained by the limitations of traditional isolation techniques [18, 19]. Generally, methods such as ultracentrifugation (UC), filtration, and size-exclusion chromatography are used to isolate these vesicles from their native biological samples [18, 19]. However, these approaches present several challenges: they are often time-consuming, retain impurities, offer limited yields, require chemical elution, as well as specialized laboratory equipment and expertise [18, 19]. Standard protocols for bacterial EV isolation typically start with ultrafiltration to remove bacterial debris, protein aggregates and other impurities. This is followed by UC steps to concentrate bacterial EVs and reduce the amount of non-bacterial EV-associated proteins, though with moderate success. In particular, isolated bacterial EVs may be contaminated with remaining bacterial flagella or large protein complexes, complicating downstream experiments and analyses [18, 19].

Building on these limitations, we have recently introduced a portable microstructured electrochemical device (PMED) for the immunoaffinity-based capture and voltage-triggered

release of EVs [20]. In our previous work, this device was used to isolate different EV subpopulations from large volumes of various mammalian biofluids, as well as from the skin wounds of both healthy and diabetic mice [20]. Compared to UC, the method allowed to isolate EVs within a considerably shorter time, with enhanced purity and selectivity, while preserving their biological activity and structural properties [20].

In this study, we investigated the performance of the device for isolating EVs from bacteria cell culture supernatants and contaminated human urine. After isolation, the collected bacterial EVs were characterized for their physicochemical and biological properties. As a proof of concept, we used *E. coli* and *Lb. fermentum* cell culture supernatants for bacterial EV isolation. The selection was strategically made to demonstrate the versatility and robustness of the device across bacterial types with distinct EV biogenesis mechanisms, surface markers and biophysical properties. Both bacterial species are clinically significant. *E. coli* EVs serve as biomarkers for urinary tract infections (UTIs) and systemic infections [17, 21], while *Lb. fermentum* EVs have potential applications in probiotic therapies and modulation of inflammatory responses [22, 23].

Materials and methods

Materials

3-Aminopropyltrimethoxysilane (S00750-5 g) was purchased from Fluorochem (UK). Mouse monoclonal anti-CD9 antibody (C-4) (sc-13118), mouse monoclonal anti-TSG101 antibody (sc-7964), were purchased from Santa Cruz Biotechnology (USA). Mouse monoclonal anti-bacterial outer membrane protein-A antibody (OMPA11-M), rabbit polyclonal anti-bacterial outer membrane protein-C antibody (BS-20213R), mouse monoclonal anti-bacterial *E. coli* elongation factor TU antibody (LS-C128699-100), rabbit polyclonal anti-bacterial flagellin antibody (316137), were purchased from Anawa CliniSciences Group (Switzerland). Rabbit polyclonal anti-bacterial surface layer protein antibody (AA 301–400) was purchased from Antibodies Online (USA). Polyclonal goat anti-mouse immunoglobulins/HRP secondary antibodies (P0447) were purchased from Dako (Denmark) and polyclonal goat anti-rabbit immunoglobulins/HRP secondary antibodies (ab97051) were purchased from abcam (CB2 0AX, United Kingdom). Phosphate buffered saline (PBS, KH_2PO_4 1 mM, NaCl 155 mM, $\text{Na}_2\text{HPO}_4 \cdot 7\text{H}_2\text{O}$ 3 mM, pH 7.4) was purchased from Thermo Fisher Scientific (USA). Silver/silver chloride paste (60/40), skim milk powder, bovine serum albumin (BSA), tris(hydroxymethyl)aminomethane (Tris) base, polysorbate

20, and ethanol absolute (>99.8%), were purchased from Sigma–Aldrich (USA). SYLGARD 184 silicon elastomeric kit was purchased from Dow Corning (USA). De-ionized water (DIW) was supplied by a Merck Millipore MilliQ Direct-Q8 (USA). All the chemicals were used as received without further purification.

Fabrication of the PMED

The PMED was fabricated as described previously [20]. Briefly, the device consists of a three-dimensional (3D) carbon electrode with a high surface area embedded in a poly(dimethylsiloxane) (PDMS)-based microchannel. The micro-carbon fiber (μ CF) electrode is constructed from Freudenberg H23 carbon paper (22 cm \times 30 cm, catalog number: 1590042, Freudenberg Performance Materials SE & Co. KG., Germany). The fluidic channel integrates silicon tubing to facilitate the flow of biosamples, which are injected using syringes. The initial step in the device assembly is the fabrication of the microchannels. Two ethanol-washed molds were used for this purpose. Double-sided adhesive carbon tape (8 mm \times 20 m, cat. AGG3939, Agar Scientific Ltd, UK) was applied to the molds, and μ CF electrodes (Freudenberg H23, 22 cm \times 30 cm, 0.15 mm thickness, cat. 1590042, Freudenberg Performance Materials SE & Co. KG, Germany) were positioned on top of the tape. For the reference electrode, a thin 3–4 mm layer of Ag/AgCl paste (60/40% m/m, 901773-50G, Sigma-Aldrich) was applied and then dried in an oven at 80 °C. Silicon tubes (1 mm inner diameter, 3 mm outer diameter, 4.5 cm length, Millipore) were inserted into the counter electrode using needles (100 Sterican \varnothing 0.90 \times 50 mm, 20 G \times 2", Braun Injekt, Germany). PDMS (50 g) and a curing agent (5 g) were mixed, creating a whitish mixture that was poured onto the molds. The sides of the molds were delimited by microscope slides (26 \times 76 \times 1 mm, Menzel X50, Thermo Fisher Scientific) covered in aluminum foil. PDMS curing occurred at 80 °C for 1 h. The two semi-channels were then carefully removed, and the electrodes were thoroughly washed with ethanol and deionized water. The resistance of the electrodes and the quality of the contacts were measured using a Digital Multimeter (UNI-T UT61E, Unitrend Technology, China). The conductivity of the working electrode and counter electrode) was approximately 3 Ω cm⁻¹.

Functionalization of the μ CF electrodes

The functionalization of the μ CF electrodes has been described in our previous publication [20]. The semi-channels with embedded μ CF electrodes were cleaned with 40 mL of ethanol and dried in a vacuum oven at 100 °C for 30 min. A radio frequency (RF) source at 60 W for 1 min,

at an oxygen gas pressure of 30 Pa (CY-P2L-B150, Zhengzhou CY Scientific Instrument Co., China), was then used to induce the formation of hydroxyl groups. Silanization was performed via gas-phase chemical adsorption of 300 μ L 3-Aminopropyldimethylethoxysilane (APDMES) for 16 h at 100 °C and 0 Pa in a covered glass Petri dish, followed by heating to 105 °C under vacuum for 2 h. The semi-channels were subsequently washed with 50 mL of ethanol and dried under vacuum at 100 °C in a vacuum oven (KVTS11, Salvis, AG., Switzerland).

PMED channel assembly

The assembly and characterization of the PMED channels were performed as described before [20]. The two semi-channels were aligned and combined to form a fluidic channel, then secured between two clear poly(methyl methacrylate) lids (105 mm \times 55 mm \times 5 mm) using six bolts and nuts. Steel needles were inserted into the PDMS to penetrate the μ CF electrodes without touching the fluidic channel and tubing. The fluidic system was flushed with 5 mL of deionized water and 5 mL of PBS. The metal needles were connected to a potentiostat (EmStat3 Blue, PalmSens BV, Netherlands).

Preparation of *E. coli* samples

The manufacture step involves the bacterial growth via successive unit operations from bacterial cell bank stored at -80 °C up to 400–600 L fermenters stage. The culture medium (200 mL) was collected at the end of the fermentation processes: optical density range 20.00–25.00, measured at 700 nm, (V-730, JASCO, Japan) with $>1.5 \times 10^{10}$ cells/mL. The culture medium was spun at 10,000 \times g for 20 min at a temperature of 4 °C (Allegra X-30R, Beckman Coulter, USA). The supernatant was then collected, filtered with 0.2 μ m pore-size filter (567–0020 reference, Rapid Flow Nalgene, Thermo Fisher Scientific) and used for subsequent EVs isolation experiments. In addition, 1 mL of sterile supernatant was plated on Tryptone Soy Agar plate (43011 reference, BioMérieux, France) and incubated for 48 h at 37 °C (IF75, Memmert, Germany) to check absence of bacteria cells.

Preparation of *Lb. fermentum* I3929 samples

Bacteria were grown via successive culture steps from bacterial cell bank stored at -80 °C up to 800–1000 mL lab scale fermenter. The culture medium (250 mL) was collected at the end of the fermentation processes (Multifors, INFORS HT, Switzerland) at optical density values of 3.00–3.50, measured at 700 nm, (NanoDropOne C, Thermo Fisher

Scientific) with $>1.0 \times 10^9$ cells/mL. The culture medium was spun at $6000 \times g$ for 30 min at 10°C (Allegra X-30R, Beckman Coulter). The supernatant was then collected, filtered with $0.2 \mu\text{m}$ pore size filters (Supor EKV membrane in mini Kleenpak capsule, KA02EKVP2S reference, PALL, USA) and used for subsequent EVs isolation experiments. The supernatant was also tested for sterility as mentioned above.

General protocol for isolation by UC

For both bacterial strains, 25 mL of supernatant were centrifuged at $110,000 \times g$ and 4°C for 60 min using an Optima XE-90 ultracentrifuge (Beckman Coulter), equipped with a Type 45 Ti Fixed-Angle Titanium Rotor. The resulting pellet was resuspended in 25 mL PBS, pooled and subjected to a second UC run under the same conditions. The final pellet was resuspended in 1 mL of PBS and stored at 4°C . After characterization, the aliquots were stored at -20°C .

Isolation of bacterial EVs from *E. coli* and *Lb. fermentum* I3929 samples with the PMED

For the isolation of EVs from *E. coli* and *Lb. fermentum* I3929 with the device, the electrodes were coated with $20 \mu\text{g}$ of the antibody, ($100 \mu\text{g}/\text{mL}$ in $200 \mu\text{L}$ PBS), using a 1-mL syringe. An empty 1-mL syringe was used at the other end of the channel to collect the solution. The antibody solution was incubated for 1 h at room temperature and transferred between the two syringes every 10 min, facilitating mixing and re-distribution of the antibodies. This dynamic flow approach helps ensuring even deposition of the antibodies on the carbon surface.

After incubation, the non-adsorbed antibody solution was removed using a 1 mL syringe, followed by washing with 5 mL of PBS to remove remaining non-bound antibodies. Then, 25 mL of *E. coli* supernatant or of *Lb. fermentum* supernatant were injected into the fluidic channel at a rate of 0.3–1 mL/s and recirculated ten times. The remaining solution was then withdrawn, and 40 mL of PBS were injected at 0.3 mL/s to remove contaminants. For the release step, 1 mL of PBS was injected and then withdrawn from the device. Before the electrochemical release, a 1-mL syringe filled with PBS was connected to one end of the device, and an empty 1 mL-syringe was connected to the other end. The device's needles were connected to a potentiostat, and a potential of -1.5 V was applied to the working electrode for 45 s while the solution was cycled back and forth through the channel for 10 times. This process was repeated with the electrical poles reversed. As a negative control, only PBS solution (no bacteria or additives) was processed using the PMED device, and no particles were detected by NTA. The

same experimental conditions described for the experiment with *E. coli* supernatant, were applied.

Preparation of *E. coli*-contaminated urine sample and isolation of bacterial EVs with the PMED

Urine (Human Urine Male, BioIVT, LOT# NMN563177, UK) biosample was stored at -80°C . The initial concentration of *E. coli* culture media was $10^7 \text{ CFU}/\text{mL}$. Given that counts as low as $10^2 \text{ CFU}/\text{mL}$ in urine can indicate an infection [24], a series of 1:10 serial dilutions was performed to progressively reduce the bacterial concentration. First, 1 mL of the $10^7 \text{ CFU}/\text{mL}$ culture was transferred into 9 mL of sterile PBS. The mixture was then thoroughly mixed. From this diluted sample, 1 mL was transferred into another tube containing 9 mL of PBS. This process was repeated until the bacterial concentration reached $10^4 \text{ CFU}/\text{mL}$. To achieve a final concentration of $10^2 \text{ CFU}/\text{mL}$ in 25 mL of urine, 0.25 mL of the $10^4 \text{ CFU}/\text{mL}$ dilution was added directly to the urine sample and mixed thoroughly. Finally, the resulting 25 mL of contaminated urine sample were introduced into the device channels without any pre-purification step, and EVs were isolated, following the protocol described in Section “Isolation of bacterial EVs from *E. coli* and *Lb. fermentum* I3929 samples with the PMED”. To exclude the presence of EVs from Gram-negative bacteria and eukaryotic cells, three devices were modified with anti-OmpA and tested with urine only. Following the application of standard electrical potential, no particles were detected by NTA.

Atomic force microscopy (AFM)

AFM topography imaging was conducted in tapping mode under ambient conditions using an AFM system from Horiba, France. Si cantilevers from AppNano (USA) with a spring constant of 2.7–44 N/m and a resonance frequency of 68–290 kHz were employed. Imaging was performed at a scan rate of 0.5–5 Hz. AFM topography images were analyzed using the open-source software Gwyddion (Version 2.49, Czech Republic) [25]. The root mean square (RMS) was calculated based on Eq. 1:

$$RMS = \sqrt{\frac{1}{N} \sum_{j=1}^N r_j^2} \quad (1)$$

Where:

- N = number of data points.
- j = index.
- $r_j = z_j - \bar{z}$, where:
 - z_j = height at a specific point j .

\bar{z} = mean height of the surface [25].

Preparation of the antibody, vesicles and antibody-vesicle complex solution on mica substrate for AFM imaging

The mica surface underwent the same functionalization treatment as the carbon fibers, which included oxygen plasma and silanization [20]. To prepare the OmpA antibody solution, 20 μL of the antibody solution were drop-cast directly from the original batch onto the mica surface and then dried at 40 °C for 48 h. For the *E. coli* EVs, 25 mL of the original supernatant were processed through UC (Section “General protocol for isolation by UC”). The resulting pellet was resuspended in 1 mL of PBS. Subsequently, 20 μL of this EV solution were drop-cast onto the mica surface and dried at 40 °C overnight. The antibody-vesicle complexes were prepared by gently mixing post-UC EVs with OmpA antibodies from their original stock solution at a volume ratio of 1:2 (EVs:OmpA), resulting in a final volume of 150 μL . The mixture was incubated at room temperature for 30 min to ensure efficient binding of the antibodies to the OmpA molecules on the EV surfaces. Following incubation, 20 μL of resulting solution were then drop-cast directly onto the mica surface and dried at 40 °C overnight.

Preparation of the antibody-vesicle complexes on device fibers for AFM imaging

To prepare the OmpA antibody-EV complex on the device fibers, the isolation procedure described in Section “Isolation of bacterial EVs from *E. coli* and *Lb. fermentum* I3929 samples with the PMED” was followed without applying electrical voltage, as the objective was to image vesicle binding to the antibodies rather than their release. After introducing 25 mL of supernatant into the antibody-modified channels and performing a PBS wash, the fibers—now containing the antibody-vesicle complexes—were carefully removed from the carbon tape using tweezers, separated, and placed on a glass substrate. The substrate was then incubated at 40 °C overnight, covered with a cup to prevent dust contamination. Once dried, the fibers were transferred onto an atomically flat mica surface and placed under the AFM microscope for imaging.

Nanoparticle tracking analysis (NTA)

NTA was used to estimate the particle concentration and the size profile of the isolated bacterial EVs. For the measurement, a ZetaView[®] PMX 120-Z instrument (Particle Metrix GmbH, Germany), featuring a 405-nm laser source and a CMOS camera, was used. The NTA device was calibrated

with a 1:500,000 dilution of silica beads. To measure our samples, the shutter was set to 150, sensitivity to 85, and the frame rate to 30. Data were analyzed with the ZetaView software version 8.04.04 SP2, (Particle Metrix GmbH), applying a bin class width of 5 nm, a minimum brightness of 25, a minimum area of 5, and a maximum area of 1000. A 1:50 (v/v) dilution of the EV samples was inserted using a syringe and measured for each sample in triplicates. The Savitzky-Golay filter (Points of Window 10) was used for smoothing data by fitting successive subsets of adjacent data points with a second-degree polynomial function. The NTA plots show the mean particle size and concentration, derived from 3 independent experiments, conducted each in triplicates.

Dynamic light scattering (DLS)

The hydrodynamic diameter (nm) and zeta-potential (mV) of the vesicles were measured on a Malvern Zetasizer Advance Pro 722 instrument (Malvern Panalytical, UK) operating at a scattering angle of 179° and at a temperature of 25 °C. The hydrodynamic diameters were determined based on light scattering intensity, with samples diluted 1:10 (v/v) PBS in nanopure water, and measured in 70 μL micro UV-cuvettes (Brand GmbH+CO. KG., Germany). The zeta-potentials were performed *via* laser Doppler anemometry, with samples diluted with 10% (v/v) PBS in nanopure water and analyzed in 800 μL Folded Capillary Zeta Cell cuvettes (Malvern Panalytical GmbH, Germany).

Transmission electron microscopy (TEM)

TEM was used to image EVs. To this end, 300-mesh copper grids with ultrathin carbon support film were negatively glow-discharged in a Pelco EasiGlow discharge system (Ted Pella Inc., USA) at 25 mA for 30 s at a pressure of 38 Pa. Subsequently, 4 μL of the EV solution were deposited onto the grids for a 30 s absorption period. The grids were treated with a uranyl acetate staining solution and washed with distilled water. Excess liquid was carefully removed using filter paper, and the grids were dried under ambient conditions. The samples were imaged with a Tecnai F20 field emission gun microscope equipped with a combination of a CCD camera (ORIOUS SC200 2 K, Gatan, USA) and a direct electron detector (Falcon II 4 K, Thermo Fisher Scientific) at an acceleration voltage of 120 kV. The micrographs were acquired in the bright field mode.

Cryo transmission electron microscopy (Cryo-TEM)

To prepare samples for cryo-TEM, lacey carbon EM grids, (Au 300 mesh, 150 μm , Byolist Scientific, USA), were

glow-discharged in Pelco EasiGlow system (Ted Pella Inc) at 25 mA for 30 s at a pressure of 38 Pa. Subsequently, 3.4 μL of the EV solution were applied onto the carbon side of EM grid, which was then blotted for 2.0 s and plunge-frozen into the precooled liquid ethane: propane mixture with Vitrobot Mark IV (Thermo Fisher Scientific). This procedure applied a thin layer of amorphous ice to the samples, preserving them in their native state and shielding them from potential radiation damage. In order to obtain a good ice thickness, the blotting time was set to 2.5 s, the blotting force to 0, and the temperature to 22 °C. The cryo-TEM images were acquired at Titan Krios FEG (Thermo Fisher Scientific) at 300 kV using a direct electron detector (Falcon III 4k \times 4k) (Thermo Fisher Scientific), which works in tandem with a Ceta 16 M 4k \times 4k CMOS detector (Thermo Fisher Scientific) and K2 (Gatan, USA) with the Quantum LS energy filter (Gatan).

Determination of bacterial EV protein concentration

The total protein content of bacterial EV samples was measured with the Micro BCA Protein Assay Kit (Thermo Fisher Scientific), according to the manufacturer's instructions. The preparation of BSA standards is described in Table S1. Bacterial EVs samples were prepared by diluting 5 μL of sample with nanopore water to a volume of 150 μL . After addition of 150 μL Micro BCA reagent (25:24:1 (v/v), reagent A:B:C) per well, the plate was incubated at 37 °C for 90 min in the dark. The absorbance was measured at 562 nm using the Tecan Infinite M200 plate reader (Tecan, Switzerland). Protein concentration was determined by accounting for the dilution of the EV sample.

Western blotting

Sample buffer (0.25 M Tris, 10% w/v SDS, 30% v/v glycerol, 0.02% w/v bromophenol blue, 5% v/v β -mercaptoethanol) was added 5:1 (v/v) to the bacterial EV samples to denature proteins and promote a sufficient flow on the gel. The samples were then heated for 5 min at 95 °C. Following this, the samples and the size marker were loaded on a 12% SDS polyacrylamide gel (total final volume loaded in each well was 15 μL). The protein samples (1–7 μg) were resolved at 80 V for approximately 1.5 h. The transfer to polyvinylidene fluoride membranes was performed with a Trans-Blot[®] Turbo[™] system at 25 V for 10 min (Bio-Rad, USA). Blocking was conducted for 2 h using Tris-buffered saline (20 mM Tris, 150 mM NaCl) with 0.1% (v/v) polysorbate 20 (TBS-T) and 5% (w/v) skim milk powder for OmpA, OmpC, flagellin, TSG101 and CD9. Instead, blocking was conducted for 2 h using 8% (w/v) BSA in tris-buffered saline (TBST) for Elongation TU, while 15% (w/v) BSA in

TBS-T was used for ENO-1 and S-layer. These conditions were optimized to minimize non-specific antibody interactions while maintaining effective target binding. Following this incubation time, the blocking solution was discarded, and the membranes were incubated with primary mouse monoclonal anti-bacterial antibodies including OmpA and Elongation TU, or with primary rabbit polyclonal anti-bacterial antibodies including OmpC, flagellin, S-layer and ENO1 in TBS-T (1:200 v/v). Primary antibodies were incubated overnight at 4 °C. After three washes with TBS-T (20 min, room temperature), secondary horseradish peroxidase (HRP)-conjugated antibodies in TBS-T were added for 4 h at 4 °C. Antibody concentrations (v/v) are provided in Table S2. Membranes were incubated with Western Blotting Luminol reagent (Santa Cruz Biotechnology, USA) according to the manufacturer's protocol and imaged using a ChemiDoc MP Imaging System (Bio-Rad).

Nano flow cytometry (NanoFCM)

Bacterial EVs were labeled with 5 μM CellTrace[™] Far Red dye (Thermo Fisher Scientific) in PBS, following a previously described protocol [26]. Briefly, samples were incubated overnight at 4 °C with the dye, followed by 15 min at 37 °C to promote acetate hydrolysis of the dye. Excess dye was removed by dialysis against PBS overnight at 4 °C using the Pur-A-Lyzer[™] Mini 6000 Dialysis Kit (Sigma-Aldrich).

Samples were analyzed using a Flow NanoAnalyzer N30 instrument (NanoFCM Co., Ltd., UK). Light scattering and fluorescence from individual particles were collected for 1 min across three channels: 488/10, 525/40, and 670/30 using single-photon counting avalanche photodiode (SPCM APD) detectors. Channel alignment was performed with fluorescent 250 nm silica QC beads and particle size was determined according to standard operating procedures by generating calibration curves using the S16M-Exo silica nanosphere cocktail (both NanoFCM Co., Ltd.), which includes four distinct silica particle populations with diameters of 68 nm, 91 nm, 113 nm and 155 nm. Samples were measured with lasers set to 10/50 mW (488 nm) and 20/100 mW (638 nm) with a 10% side scatter decay. The sampling pressure was maintained at 1.0 kPa throughout the measurement. Before measurement, the samples were diluted in PBS to ensure a final event count ranging from 500 to 3200. The data was processed using the NanoFCM Professional Suite (version 2.3, NanoFCM Co., Ltd.) and the FlowJo software (version 10.9.0, BD Biosciences, USA). Experimental data are shown as a result of 3 independent experiments, conducted each in triplicates.

Proteomic analysis—EVs proteome analysis

Two *Lb fermentum* EV samples (post-device) were dissolved in 1% (w/v) sodium deoxycholate in 50 mM ammonium bicarbonate buffer (pH 8), reduced with 1 mM dithiothreitol, and alkylated using 5.5 mM iodoacetamide for 10 min at room temperature. Proteins were in-solution digested with trypsin (Promega, USA). Sodium deoxycholate was precipitated using 50% TFA (trifluoroacetic acid), and tryptic peptides were purified by STAGE tips prior to LC–MS/MS measurements. These were performed on a QExactive HF-X mass spectrometer (Thermo Fisher Scientific) coupled to an EasyLC 1000 nanoflow-HPLC (Thermo Fisher Scientific). Peptides were separated on a fused silica HPLC-column tip (I.D. 75 μ m, New Objective, self-packed with ReproSil-Pur 120 C18-AQ, 1.9 μ m (Dr. Maisch, Germany) to a length of 20 cm), using a gradient of A (0.1% v/v formic acid in water) and B (0.1% v/v formic acid in 80% v/v acetonitrile in water). The mass spectrometer was operated in data-independent mode. After each survey scan (mass range $m/z=350$ – 1200 ; resolution: 120,000), 28 DIA scans with an isolation width of 31.4 m/z were performed, covering a precursor range of 350 to 1200 m/z . AGC target value was set to 3×10^6 , resolution to 30,000, and normalized collision energy to 27%. Data were analyzed using Spectronaut software version 15.7 (Biognosys, Switzerland) with standard settings (without imputation) in direct DIA mode, using the reference proteomes uniprotkb_ *Limosilactobacillus fermentum* and uniprotkb_Rabbit (UniProt, full length) and common contaminants.

Cell stimulation assays

HEK-Blue™ hTLR2: hkb-htr2 and HEK-Blue™ hTLR4: hkb-htr4 (Invivogen, USA) were plated at a density of 5.10^4 cells / well of a 96 well plate in 100 μ L of culture medium (DMEM high glucose glutamax, Gibco, 61965-026 + 10% v/v fetal calf serum, Gibco A52567, 10% fetal bovine serum (FBS), Thermo Fisher Scientific). After 24 h of incubation, the medium was replaced with fresh medium, and various dilutions of EVs isolated from *Lb. fermentum* culture supernatant were added to the cells. After 24 h of incubation 37 °C under 5% CO₂ atmosphere, SEAP activity was revealed using QUANTI-Blue reagent (Invivogen) and a Fluorescence plate reader (SpectraMax M3, Molecular Devices, USA) according to manufacturer's instruction. Results were expressed by comparison between the basal Optical Density (OD) measured in cells supernatant without any treatment and OD obtained after cells stimulation. The NF- κ B activity was calculated using Eq. 2

$$NF - \kappa B \text{ activity} = \frac{\text{OD of stimulated cells}}{\text{OD of cell cultured with medium}} \quad (2)$$

This ratio was expressed as activity “relative to unstimulated cells”; a ratio equal to 1 corresponding to absence of NF- κ B activity.

Statistical analysis

The statistical analysis was conducted using the GraphPad Prism software version 8.0.0, (GraphPad Software, Inc., USA). The data were presented as mean \pm SD. p-values were calculated using an unpaired t-test with a two-tailed distribution and unequal variance. * $p < 0.05$, ** $p < 0.01$, *** $p < 0.001$, **** $p < 0.0001$.

Results and discussion

AFM imaging of the antibody-vesicle interaction

The PMED operates via a dual mechanism of EV capture through immunoaffinity and subsequent release triggered by electrical voltage (Fig. 1A-E). As previously described, the system comprises a fluidic channel featuring antibody-coated microstructured carbon electrodes (Fig. 1A-B) [20]. During operation, the biological sample flows through the channel (Fig. 1C), enabling selective capture of EVs by immunoaffinity. This process isolates EVs from the rest of the sample components, which are subsequently removed by washing with PBS (Fig. 1D). Finally, the captured EVs are released into PBS using a -1.5 V electrical voltage (Fig. 1E), and stored at 4 °C for a short period prior to downstream characterization. Three main processes contribute to the release of the EVs from the antibodies: (I) Electrical repulsion between the negatively charged EVs and the negative working electrode (WE). (II) Below -1.23 V, water molecules are subjected to electrolysis, which produces H₂ (g) and O₂ (g) on the surface of the WE and the counter electrode (CE), respectively. These gases repel the EVs and prevent re-binding. (III) Local pH changes on the surface of the electrodes lead to conformational changes of the antibodies and weaken their affinity towards the EVs [20].

To isolate bacterial EVs from *E. coli* culture media, the device's carbon electrodes were coated with an anti-OmpA antibody. OmpA is a porin, which is abundant in the outer membrane of many Gram-negative bacteria, including *E. coli*. It facilitates the passive diffusion of small molecules, like amino acids, across the membrane and plays a crucial role in maintaining membrane integrity [27, 28].

AFM was used to confirm and visualize the specific binding interactions between the captured *E. coli* vesicles and anti-OmpA antibodies on the carbon fiber (Fig. 1F-H). To allow vesicle-antibody binding, the *E. coli* culture medium was introduced into the device, where the carbon

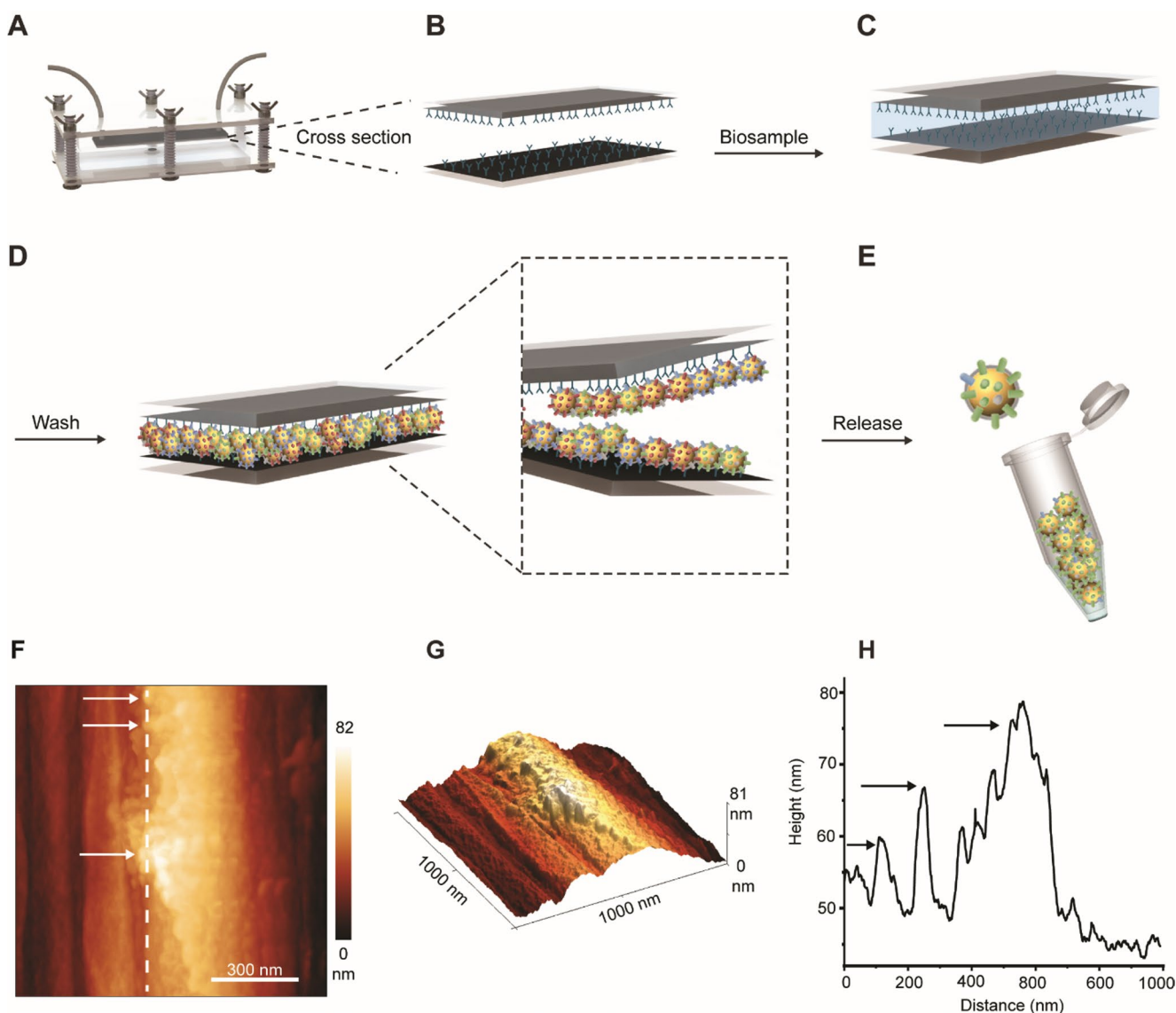


Fig. 1 (A–E) Schematic representation of the PMED and operation process. (A) PMED setup, (B) antibody conjugation of the electrodes, (C) injection of the sample, (D) washing step and (E) controlled release of the attached EVs through the application of voltage. (F) AFM topography image of a carbon fiber incubated with *E. coli*-derived EV- anti-OmpA antibody complexes attached on top (after step D of the process). Area: $1 \mu\text{m}^2$. Resolution: 516×516 pixels. (G)

electrodes were coated with anti-OmpA antibodies (Section “Preparation of the antibody-vesicle complexes on device fibers for AFM imaging”). After passing the *E. coli* culture medium through the channels, the carbon fibers were carefully removed from the carbon tape. They were then dried at 40°C on a clean glass substrate overnight before being transferred to an atomically flat mica surface for analysis. The coated fibers were compared with 5 control samples: mica substrate, pristine carbon fibers, OmpA antibodies on the mica substrate, EVs isolated via UC on the mica substrate, OmpA antibody-EV complexes on the mica substrate

3D representation of the AFM topography image shown in Panel F), displaying the presence of *E. coli*-derived EV- anti-OmpA antibody complexes on the carbon fiber surface. (H) Height profile of the carbon fiber surface along the line marked in Panel F). The arrows in Panels F) and H) indicate the location of the *E. coli*-derived EV- anti-OmpA antibody complexes on the carbon fiber

(Fig. S1 and Section “Preparation of the antibody, vesicles and antibody-vesicle complex solution on mica substrate for AFM imaging”). AFM imaging of individual antibodies on carbon fibers was not feasible due to the substantial intrinsic roughness of the fiber surface.

As shown in Fig. S1A–N, similar height was observed for the antibody-EV complexes on the carbon fibers and those on the mica substrate, suggesting successful imaging of the complexes on the fibers. In particular, the AFM topography image (Fig. 1F) and its corresponding 3D representation (Fig. 1G) revealed several globular features on the

surface of the coated carbon fibers. The height profile along the fiber, presented in Fig. 1H, indicates that the globular features attain a height of up to 30 nm, consistent with the maximum height of the EV-protein complexes observed on the mica substrate (Fig. S1G and H). In contrast, the AFM topography image of a pristine carbon fiber (without antibodies and EVs) showed no globular features (Fig. S1I). The RMS roughness of the topography image of the carbon fiber incubated with the antibody-EV complexes (Fig. 1F) was 17.7 nm, whereas the uncoated fiber exhibited an RMS roughness of 8.4 nm (Fig. S1J). Additional AFM measurements of the carbon fibers incubated with the antibody-EV complexes revealed RMS roughness of 12.1 nm and 14.0 nm (Fig. S1K and S1M). These results confirm successful capture of the *E. coli*-derived EV-protein complexes by the carbon fibers.

Isolation of bacterial EVs from Gram-negative *E. coli* and Gram-positive *Lb. fermentum*

As described above, the electrode surfaces were coated with anti-OmpA antibodies to isolate bacterial EVs from the Gram-negative *E. coli* culture medium. For *Lb. fermentum*, an anti-S-layer antibody was used to capture the corresponding bacterial EVs, taking advantage of its presence on the outer membrane of *Lactobacillus* species. S-layer glycoproteins self-assemble into a uniformly spaced pattern on the bacterial cell surface, where they play a key role in adhesion to intestinal epithelial cells and the mammalian extracellular matrix [29].

For both types of experiments, EVs were isolated in triplicates using either the device or UC, collected in PBS and subsequently characterized (Figs. 2 and 3, Fig. S2, S3, S5 and Table S3). Following isolation with the device, NTA revealed mean particle diameters of 107.3 ± 2.8 nm for *E. coli*-derived EVs, and 140.7 ± 10.6 nm for *Lb. fermentum*-derived EVs, with concentrations of 1.6×10^{11} and 1.9×10^8 particles/mL, respectively (Fig. 2A, and 3A). With UC, the mean diameters were 104.2 ± 14.7 nm for *E. coli*-derived EVs and 138.8 ± 9.4 nm for *Lb. fermentum*-derived EVs, with concentrations of 1.2×10^{11} and 1.6×10^9 particles/mL, respectively (Fig. S2A, S3A). Overall, the mean particle diameters were comparable between the two isolation methods, whereas the particle size distribution was notably broader in the UC-isolated samples vs. the device. This discrepancy may be due to a higher presence of contaminants, such as protein aggregates and cell debris, retained during the UC process. DLS analysis revealed comparable size values (~ 120 – 130 nm) for EVs isolated using the device and UC (Fig. S5A, Table S3). In contrast, the zeta potential values differed between the two methods, possibly reflecting the presence of additional impurities (Fig. S5B, Table S3).

The less negative zeta potential observed in EVs isolated from *Lb. fermentum* compared to those from *E. coli* could be attributed to differences in cell wall structure and composition. EVs derived from Gram-negative bacteria, such as *E. coli*, are characterized by the presence of abundant LPS on their membranes [1, 2, 11]. LPS carry a high negative charge due to phosphate groups and other negatively charged moieties that contribute to the more negative zeta potential of *E. coli*-derived EVs. EVs from Gram-positive bacteria, such as *Lb. fermentum*, lack LPS but contain lipoteichoic acid [30]. While LTA contributes to the negative charge of *Lb. fermentum*-derived EVs, its effect is less pronounced than LPS [31]. TEM micrographs of the device- and UC-isolated EVs revealed a field of spherical vesicles (Figs. 2B and C and 3B and C, Fig. S2B, C and Fig. S3B, C), with the distinctive cup-shaped morphology observable at low magnification. The cup-shaped morphology was less pronounced in Gram-positive EVs, possibly due to their thicker outer layer or the reduced staining efficiency, which may lead to poor dehydration of the vesicles [32]. The phospholipid bilayer membrane structure was clearly visualized in cryo-TEM images (Figs. 2D and 3D, Fig. S2D). The cryo-TEM image of the *Lb. fermentum* sample collected post UC was heavily contaminated with proteins and/or cell debris, obscuring the grid and preventing clear visualization. Next, protein profiling was performed by Western blot analysis (Figs. 2E and 3E). For *E. coli*-derived EVs, the surface porins OmpA and OmpC, as well as the cytosolic protein elongation factor TU (EF-TU), were detected (Fig. 2E). The latter has the function to shuttle aminoacylated tRNAs to the ribosome during protein translation [18, 33]. Although initially predicted to be predominantly expressed in the bacterial cytoplasm, EF-TU has also been detected in OMVs from various *E. coli* strains [33, 34]. In contrast to UC, the bacterial EV sample isolated with the device barely showed any flagellin, a contaminating protein marker, suggesting higher purity of the isolated sample [18]. During bacterial culture or sample processing, small amounts of OmpA proteins may be released from cell debris or disrupted vesicles. Therefore, we performed Western blot analysis on the collected supernatant, as a control experiment. However, no detectable bands were observed for these proteins in the supernatant samples, suggesting that their concentrations were below the detection limit of Western blotting (Fig. S7).

For *Lb. fermentum*-derived EVs, Western blot analysis revealed the presence of S-layer and enolase-1 (ENO1) (Fig. 3E). ENO1 is a multifunctional protein that primarily serves as a glycolytic enzyme in the cytosol, catalyzing the conversion of 2-phospho-D-glycerate to phosphoenolpyruvate during aerobic glycolysis [35]. It is found both as a cytoplasmic and a surface-associated protein in many Gram-positive bacteria and their derived EVs [36, 37].

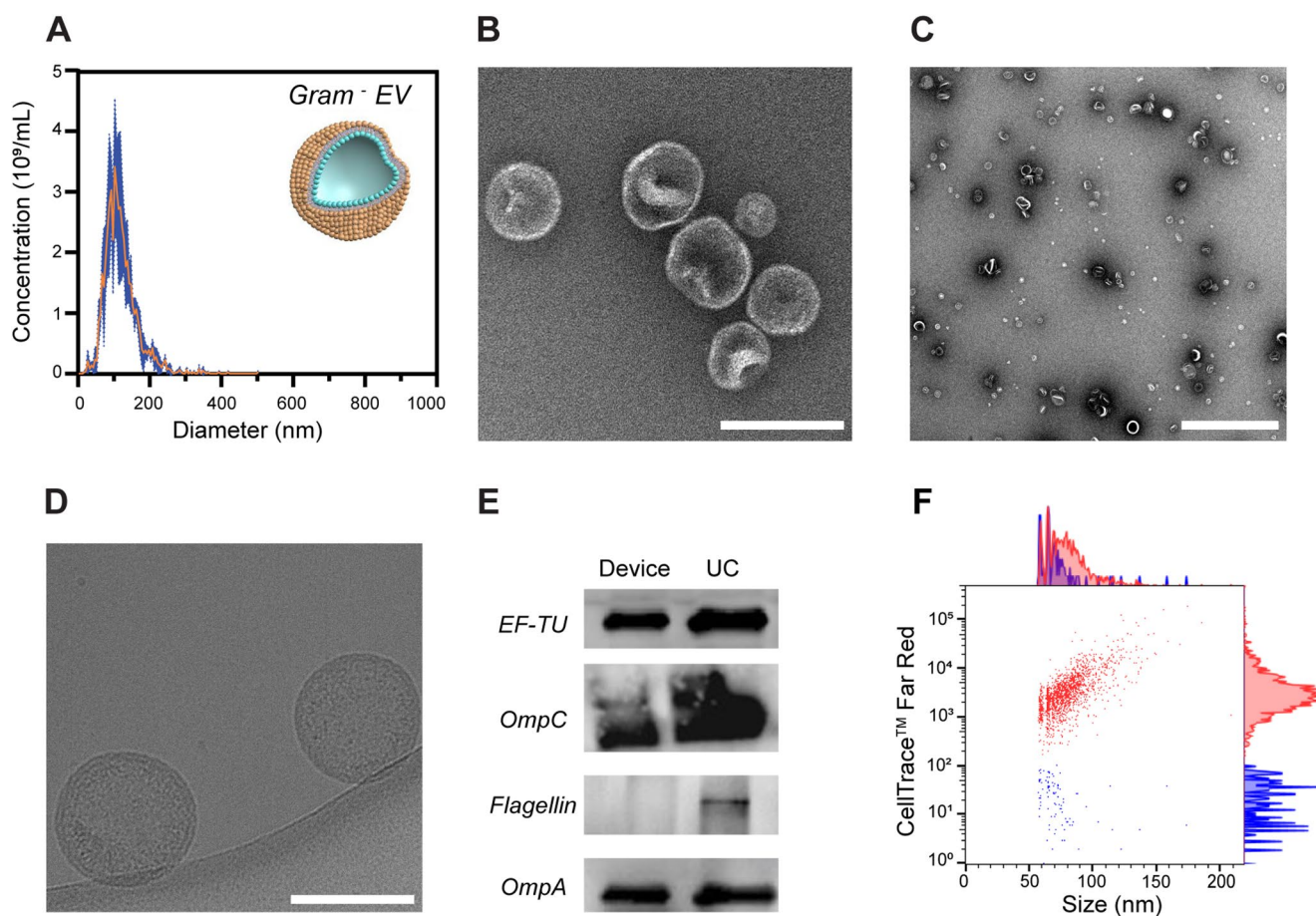


Fig. 2 Characterization of bacterial EVs from Gram-negative *E. coli* supernatant. **(A)** NTA plot of EVs isolated using the device with an anti-OmpA antibody coating. Experimental data are expressed as mean (orange) \pm SD (dark blue) ($n = 3$) Inset: schematic representation of a Gram-negative EV with the outer membrane colored in gold. **(B)** Representative high magnification TEM image of a field of isolated EVs in PBS. Scale bar: 200 nm. **(C)** Representative low magnification TEM image of a field of isolated EVs in PBS. Scale bar: 500 nm. **(D)** Representative high magnification cryo-TEM image of two isolated EVs in PBS. Scale bar: 200 nm. **(E)** Western blot analysis of bacterial EV pro-

tein markers (EF-TU, OmpC, flagellin and OmpA), showing the EV proteins isolated with the device in the left lane, and those isolated by UC in the right lane. **(F)** NanoFCM analysis of CTFR stained *E. coli*-derived EVs. A representative bivariate dot plot of size (nm, x axis) vs CTFR (y axis) shown, with corresponding histograms displayed alongside. CTFR-positive events are shown in red, while CTFR-negative events are shown in blue. A representative plot is reported, with the mean values of $91.9 \pm 2.8\%$ for CTFR-positive events and $8.1 \pm 2.8\%$ for CTFR-negative events. Original uncropped Western blots are provided in the supporting information (Fig. S6)

Unlike UC, a faint band corresponding to the contaminant flagellin was observed in the bacterial EV sample isolated using the device method. This contaminant might eventually be removed by optimizing the washing step [20]. NanoFCM was used to further validate the presence of bacterial EVs in all collected samples (Figs. 2F and 3F, Fig. S2E, F, S3D, E). To this purpose, bacterial EVs were labeled with CellTrace™ Far Red (CTFR) dye. After staining the samples isolated with the electrochemical device, $91.9 \pm 2.8\%$ of events in *E. coli*-derived EVs and $84.8 \pm 9.5\%$ of events in *Lb. fermentum*-derived EVs were positive for CTFR staining, suggesting that the majority of detected particles were EVs. Finally, a pilot classical bottom-up proteomics analysis coupled to label-free quantification of fragment spectra based on Data-Independent-Analysis (DIA) was performed

to characterize the proteomes of isolated vesicles. Data were analyzed against a *Limosilactobacillus fermentum* and rabbit database, confirming no IgG was identified in the samples.

Taken together, these results confirm that EVs were isolated from the medium of *E. coli* and *Lb. fermentum* bacterial cells using our electrochemical device.

Isolation of bacterial EVs from Gram-negative *E. coli* contaminated urine sample

Urinary EVs provide valuable insights into the health of the urinary system, particularly the functionality of podocytes and renal tubular cells [38]. Urine, which can be collected easily, frequently, and in large quantities through noninvasive methods, is an ideal fluid for biomarker analysis [38].

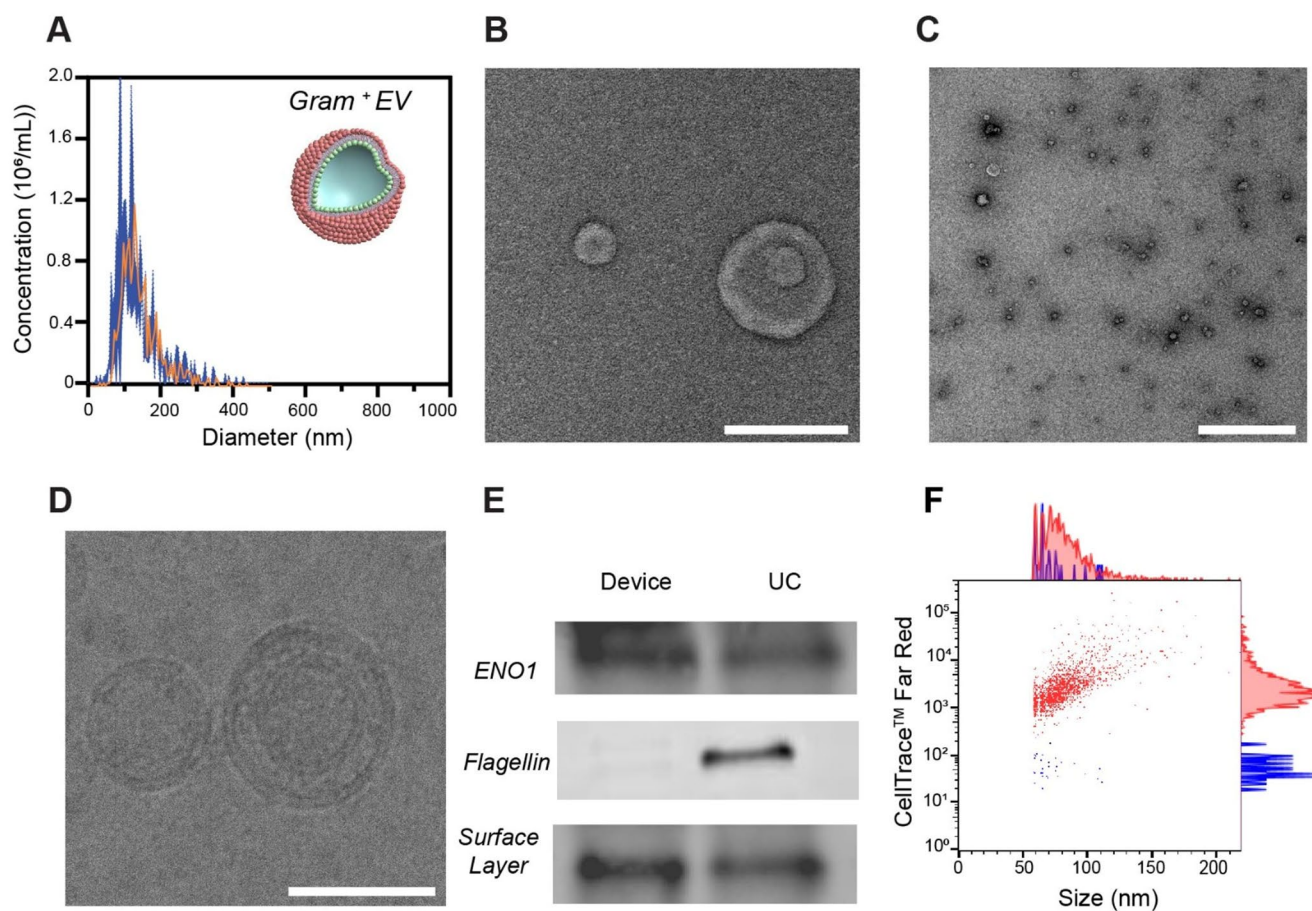


Fig. 3 Characterization of bacterial EVs from Gram-positive *Lb. fermentum* supernatant. **(A)** NTA plot of EVs isolated using the device with an anti-S-layer antibody coating. Experimental data are expressed as mean (orange) \pm SD (dark blue) ($n = 3$). Schematic representation of a Gram-positive EV with the cytoplasmic membrane colored in rose pink. **(B)** Representative high magnification TEM image of isolated EVs in PBS. Scale bar: 100 nm. **(C)** Representative low magnification TEM image of isolated EVs in PBS. Scale bar: 1000 nm. **(D)** Representative high magnification cryo-TEM image of two isolated EVs in PBS. Scale bar: 100 nm. **(E)** Western blot analysis of bacterial EV pro-

tein markers (ENO1, flagellin and S-layer), showing the EV proteins isolated with the device in the left lane, and those isolated by UC in the right lane. **(F)** NanoFCM analysis of CTFR stained *Lb. fermentum*-derived EVs. A representative bivariate dot plot of size (nm, x axis) vs CTFR (y axis) is shown, with corresponding histograms displayed alongside. CTFR-positive events are shown in red, while CTFR-negative events are shown in blue. A representative plot is reported, with the mean values of $84.8 \pm 9.5\%$ for CTFR-positive events and $15.2 \pm 9.5\%$ for CTFR-negative events. Original uncropped Western blots are provided in the supporting information (Fig. S6)

However, its complex composition—including proteins, salts, urea, and various metabolites—can dilute EVs and obscure key biomarkers. *E. coli*, a bacterium normally residing in the gastrointestinal tract, can migrate into the urinary system and cause UTIs [24]. Although there exist established diagnostic methods for UTIs, isolating bacterial EVs could provide complementary information, offering deeper insights into infection mechanisms and disease progression. As a proof of concept, we evaluated the device for its ability to isolate *E. coli*-derived EVs from urine (Fig. 4). *E. coli* was spiked into the urine sample to achieve a concentration of 10 CFU/mL, which falls within the typical bacterial load associated with UTIs [24]. The samples were processed with the device or UC and analyzed as described above (Fig. 4, S4, S5, Table S3). As for the isolation of vesicles

from the culture medium, EVs collected with the device from urine had an average diameter of 126.2 ± 1.8 nm and 124.6 ± 4.5 nm, as shown by NTA and DLS, respectively (Fig. 4, Fig. S5 and Table S3). Instead, EVs isolated with UC from urine showed an average diameter of 145.2 ± 6.0 nm and 175 ± 30.2 nm, as reported by NTA and DLS, respectively, (Fig. S4, Fig. S5 and Table S3). The particle concentration was found to be 2.8×10^{10} particles/mL, similar to the concentration value of 3.3×10^{10} particles/mL after isolation with UC. NanoFCM also revealed a mean value of $89.2 \pm 2.8\%$ of the events to be positive for CTFR, while a mean value of $10.8 \pm 2.8\%$ to be negative for CTFR (Fig. 4).

Similar to the results from the cell culture media, the device outperformed UC in efficiently isolating EVs. Western blot analysis of the samples (Fig. 4E) indeed revealed

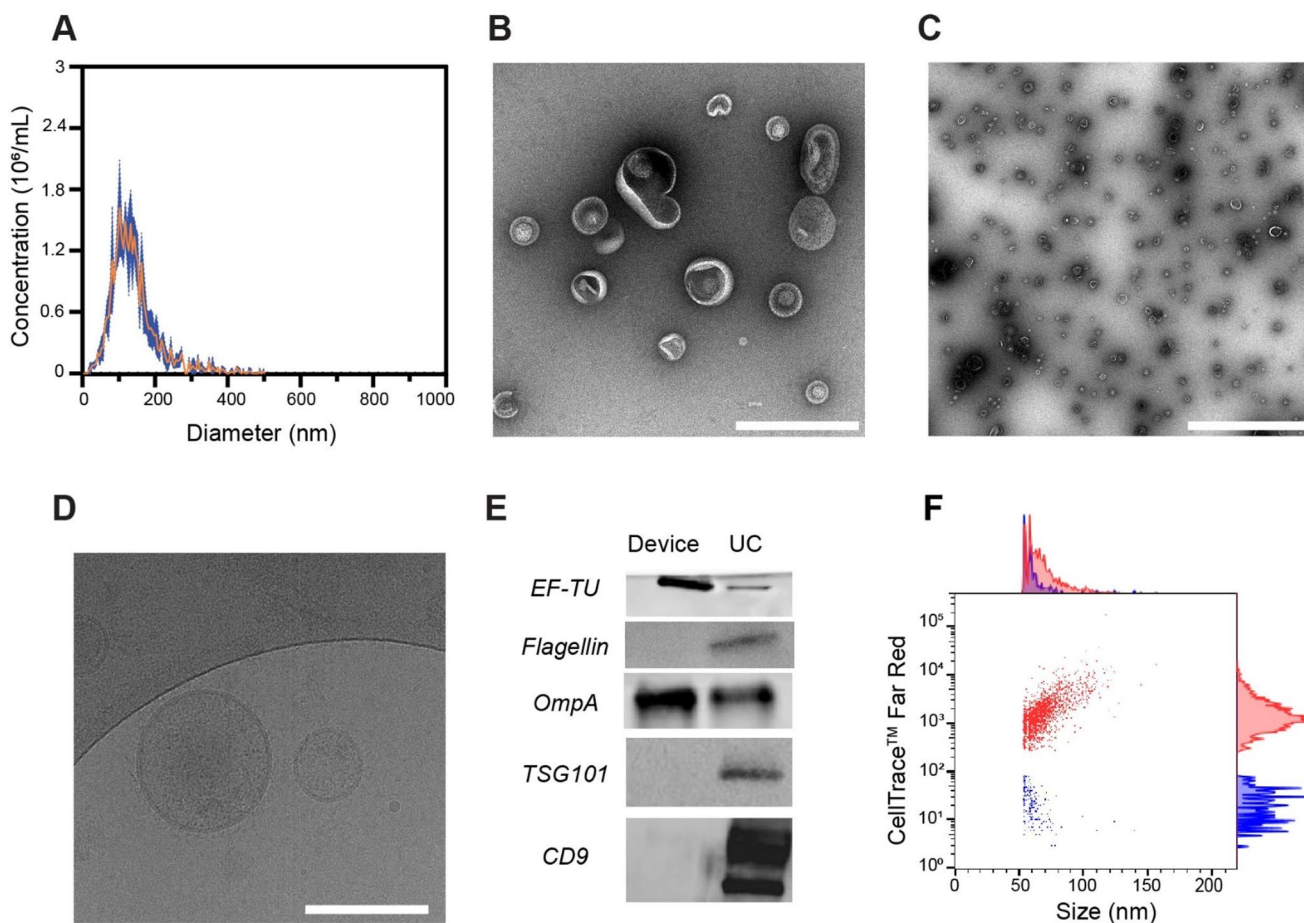


Fig. 4 Characterization of bacterial EVs from Gram-negative *E. coli* contaminated urine sample. **(A)** NTA plot of EVs isolated from patient-derived urine samples, using the device with an anti-OmpA antibody coating. Experimental data are expressed as mean (orange) \pm SD (dark blue) ($n = 3$). **(B)** Representative high magnification TEM image of a field of isolated EVs in PBS. Scale bar: 200 nm. **(C)** Representative low magnification TEM image of a field of isolated EVs in PBS. Scale bar: 1000 nm. **(D)** Representative high magnification cryo-TEM image of two isolated EVs in PBS. Scale bar: 100 nm. **(E)** Western blot analysis of bacterial EV protein markers (EF-TU, flagellin, OmpA), and of

human EV protein markers (TSG101, CD9), showing the EV proteins isolated with the device in the left lane, and those isolated with UC in the right lane. **(F)** NanoFCM analysis of CTFR stained EVs from *E. coli* contaminated urine sample. A representative bivariate dot plot of size (nm, x axis) vs CTFR (y axis) is shown, with corresponding histograms displayed alongside. CTFR-positive events are shown in red, while CTFR-negative events are shown in blue. A representative plot is reported, with the mean values of $89.2 \pm 2.8\%$ for CTFR-positive events and $10.8 \pm 2.8\%$ for CTFR-negative events. Original uncropped Western blots are provided in the supporting information (Fig. S6)

that, in contrast to UC, which co-isolated both human and bacterial EVs from contaminated urine samples (detecting human EV markers such as TSG101 and CD9 alongside bacterial markers like EF-TU and OmpA), the electrochemical device was more selective, with reduced contamination from human EVs and the flagellin marker. This feature is essential for clinical diagnostics, as the ability to distinguish between bacterial and host EVs can provide valuable insights into the diagnosis and progression of infections [39].

Isolated *Lactobacillus fermentum*-derived EVs activate TLR4 pathway

Lactic acid-producing bacteria are widely recognized for their probiotic benefits, including bolstering the host's immune system, enhancing feed digestibility, and mitigating metabolic disorders [22, 23]. *Lb. fermentum* is a Gram-positive bacterium within the *Lactobacillus* genus, known for its ability to boost immune responses and help prevent gastrointestinal and upper respiratory infections [22, 23]. In a pilot experiment, we evaluated whether the bacterial EVs isolated from *Lb. fermentum* supernatant, using the PMED and UC, were able to selectively modify the expression of negative regulators of Toll-like receptor 4 or 2 (TLR4 or TLR2) signaling in HEK-TLR4 and HEK-TLR2 reporter

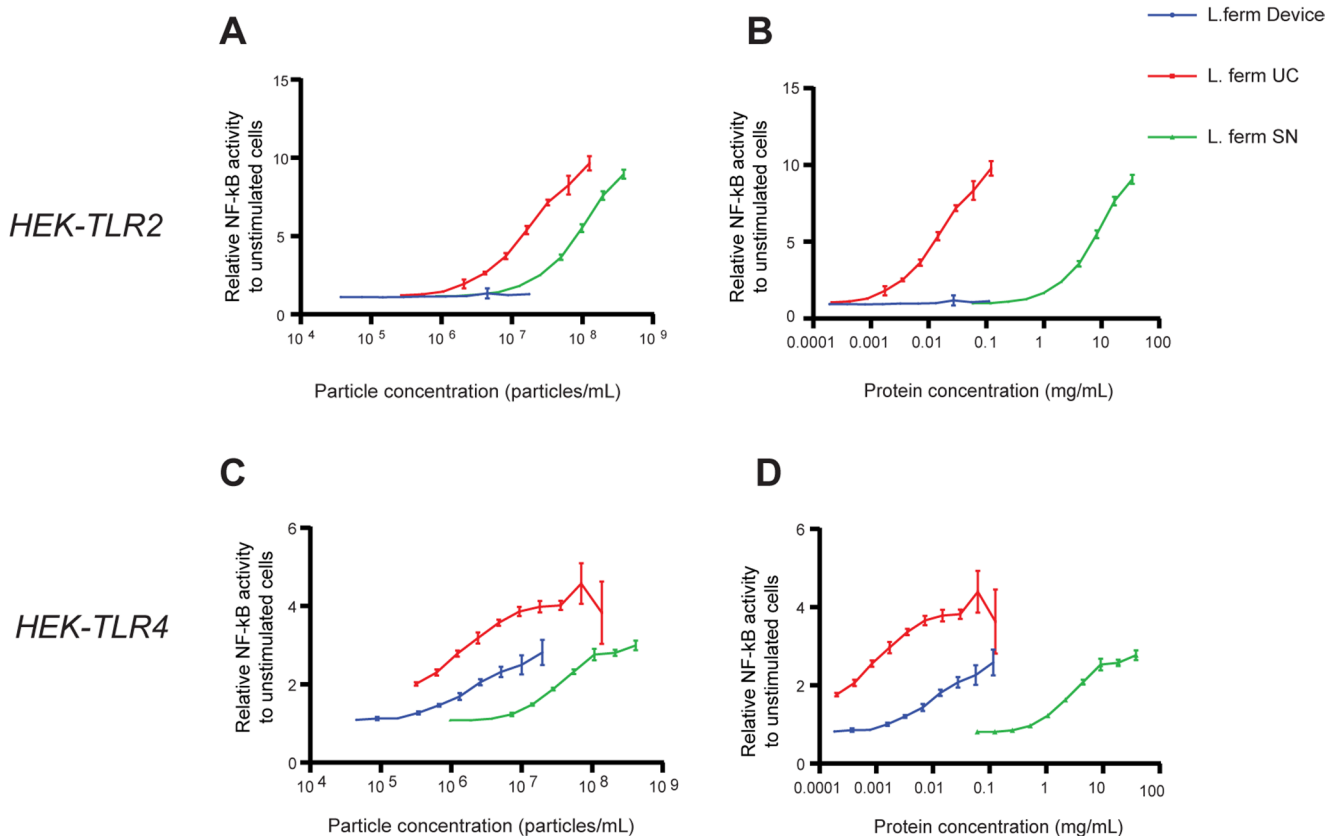


Fig. 5 Assessment of NF- κ B activity in HEK-TLR2 and HEK-TLR4 reporter cells in response to *Lb. fermentum* I3929 bacterial EVs, as a function of: (A) EV particle concentration (particles/mL) and (B) EV protein concentration (mg/mL) in HEK-TLR2 cells; (C) EV particle

concentration (particles/mL) and (D) EV protein concentration (mg/mL) in HEK-TLR4 cells. Reporter cells were stimulated for 24 h at 37 °C. Mean \pm SD ($n=4$, technical replicates), SN=*Lb. fermentum* supernatant

cell lines, respectively. To this end, the cells were incubated with UC- or device-isolated EVs, or native fermentation supernatant for 24 h. NF- κ B activation was quantified by measurement of the secreted embryonic alkaline phosphatase (SEAP) activity (Fig. 5). *Lb. fermentum* fermentation supernatant was shown to induce TLR4 and TLR2 signaling in HEK-TLR4 and HEK-TLR2 reporter cell lines, respectively, indicating the presence of TLR2 and TLR4 agonists secreted by *Lb. fermentum* during fermentation (Fig. 5).

The bacterial EVs collected with the device did not induce activation of TLR2 (Fig. 5A-B), yet they were capable of stimulating TLR4 in this HEK reporter system (Fig. 5C-D). In contrast, the UC-isolated EVs indiscriminately activated both TLR4 and TLR2, more potently than the native *Lb. fermentum* supernatant. This differential activation may stem from the absence of TLR2-activating components in device-isolated EVs, whereas UC isolation likely retains additional bacterial fragments that also engage TLR2. In this respect, in Gram-positive bacteria, TLR2-mediated recognition of PAMPs, such as LTA and PGN, triggers downstream signaling through MyD88, ultimately leading to NF- κ B activation. The absence of TLR2 activation in device-isolated

EVs suggests that the composition of the EV subset preferentially supports TLR4 engagement and/or LTA and PGN are lower in content compared to UC [40]. Proteomics and lipidomics analyses would, in the future, be essential to uncover the compositional differences between bacterial EV samples isolated using the device vs. UC.

Overall, our results highlight the ability of the PMED in isolating functionally distinct bacterial EV populations, providing a more targeted approach to studying immune responses.

Conclusion

In this study, EVs from Gram-negative (*E. coli*) and Gram-positive (*Lb. fermentum*) bacterial supernatants were isolated with an electrochemically controlled device. This device addresses key limitations of traditional methods like UC, such as contamination and limited selectivity. By combining immunoaffinity-based EV capture with voltage-driven release, the device achieves enhanced selectivity, and reduced contaminants compared to conventional techniques.

This isolation method creates avenues for biomarker discovery in liquid diagnostics and the targeted modulation of immune responses. Furthermore, the versatile antibody-conjugation strategy broadens the device's applicability to a wide range of bacterial and non-bacterial sources. For instance, beyond the previously reported isolation of mammalian EVs [20], future studies could explore its use in isolating EVs from plant-derived samples. Such applications may provide insights into plant-microbe interactions, crop improvement strategies, or the role of plant EVs in stress responses.

Supplementary Information The online version contains supplementary material available at <https://doi.org/10.1007/s13346-025-01954-1>.

Acknowledgements The authors thank Miroslav Peter and Stephan Handschin, ScopeM, ETH Zürich, for support and assistance with TEM and Cryo-EM imaging, Dr. Philipp Schätzle, Cytometry Facility of the University of Zürich (UZH), for support with the operation of NanoFCM, and Dr. Johannes Bader Dr. Marilena Bohley Steiger, and Dr. Adva Krivitsky for critical discussions on the execution of western blotting.

Author contributions VM: Performed the majority of the experiments, interpreted the data, prepared figures, and wrote the manuscript. SB: Performed AFM experiments, interpreted data, contributed to figure preparation, and participated in manuscript drafting and revision. FB: Conducted NanoFCM experiments, interpreted data, and contributed to manuscript drafting and revision. EB: Provided bacterial supernatant, supervised in vitro experiments, interpreted data, and revised the manuscript. MR: Supplied bacterial supernatants and contributed to manuscript revision. NZ: Assisted with experiments, interpreted data, prepared figures, and revised the manuscript. SH: Assisted with experiments, interpreted data, and contributed to manuscript revision. NK and RZ: Interpreted AFM data and participated in manuscript revision. SS and JD: Performed proteomics measurements and analyzed the data. JC: Conceived the study, supervised the project, interpreted data, co-wrote the manuscript, and provided the funding. VK: Conceptualized and provided the devices, interpreted data, and revised the manuscript.

Funding Open access funding provided by Swiss Federal Institute of Technology Zurich. This work was financially supported by ETH Zürich.

Data availability The data supporting the findings of this study will be available in the ETH Research Collection at <https://www.research-collection.ethz.ch>.

Declarations

Declaration of conflict of interest V.K. and J.-C.L. have filed a patent application related to this work. V.K. is founder of Acytronix GmbH, a company commercializing the device. The other authors declare no competing interests.

Ethics approval Not applicable.

Consent to participate Not applicable.

Consent to publish Not applicable.

Open Access This article is licensed under a Creative Commons Attribution 4.0 International License, which permits use, sharing, adaptation, distribution and reproduction in any medium or format, as long as you give appropriate credit to the original author(s) and the source, provide a link to the Creative Commons licence, and indicate if changes were made. The images or other third party material in this article are included in the article's Creative Commons licence, unless indicated otherwise in a credit line to the material. If material is not included in the article's Creative Commons licence and your intended use is not permitted by statutory regulation or exceeds the permitted use, you will need to obtain permission directly from the copyright holder. To view a copy of this licence, visit <http://creativecommons.org/licenses/by/4.0/>.

References

- Schwechheimer C, Kuehn MJ. Outer-membrane vesicles from Gram-negative bacteria: biogenesis and functions. *Nat Rev Microbiol.* 2015;13:605–19. <https://doi.org/10.1038/nrmicro3525>.
- Hosseini-Giv N, Basas A, Hicks C, El-Omar E, El-Assaad F, Beheshti EH. Bacterial extracellular vesicles and their novel therapeutic applications in health and cancer. *Front Cell Infect Microbiol.* 2022;12:962216. <https://doi.org/10.3389/fcimb.2022.962216>.
- Mandal PK, Ballerin G, Nolan LM, Petty NK, Whitchurch CB. Bacteriophage infection of *Escherichia coli* leads to the formation of membrane vesicles via both explosive cell lysis and membrane blebbing. *Microbiol.* 2021;167:001021. <https://doi.org/10.1099/mic.0.001021>.
- Junhua X, Qiqiong L, Nie S. Bacterial extracellular vesicles: an emerging postbiotic. *Trends Food Sci Technol.* 2024;143:104275. <https://doi.org/10.1016/j.tifs.2023.104275>.
- Bose S, Aggarwal S, Singh DV, Acharya N. Extracellular vesicles: an emerging platform in gram-positive bacteria. *Microb Cell.* 2020;7:312. <https://doi.org/10.15698/mic2020.12.737>.
- Bitto NJ, Chapman R, Pidot S, Costin A, Lo C, Choi J, D'Cruze T, Reynolds EC, Dashper SG, Turnbull L, Whitchurch CB, Stinear TP, Stacey KJ, Ferrero RL. Bacterial membrane vesicles transport their DNA cargo into host cells. *Sci Rep.* 2017;7:7072. <https://doi.org/10.1038/s41598-017-07288-4>.
- Kumari P, Wright SS, Rathinam AV. Role of extracellular vesicles in immunity and host defense. *Immunol Invest.* 2024;53:10–25.
- Wu Q, Li Z, Kan J, Liu Q, Fu C, Zhang Y, Liu X, Du J. Insights into the unique roles of extracellular vesicles for gut health modulation: mechanisms, challenges, and perspectives. *Curr Res Microb Sci.* 2024;7:100301. <https://doi.org/10.1016/j.crmicr.2024.100301>.
- Molina-Tijeras AJ, Gálvez J, Rodríguez-Cabezas ME. The Immunomodulatory properties of extracellular vesicles derived from probiotics: A novel approach for the management of Gastrointestinal diseases. *Nutr.* 2019;11:1038. <https://doi.org/10.3390/nu11051038>.
- Asong J, Wolfert MA, Maiti KK, Miller D, Boons GJ. Binding and cellular activation studies reveal that Toll-like receptor 2 can differentially recognize peptidoglycan from Gram-positive and Gram-negative bacteria. *JBC.* 2009;284:8643–53. <https://doi.org/10.1074/jbc.M806633200>.
- Peregrino ES, Castañeda-Casimiro J, Vázquez-Flores L, Estrada-Parra S, Wong-Baeza C, López JS, Wong-Baeza I. The role of bacterial extracellular vesicles in the immune response to pathogens,

- and therapeutic opportunities. *Int J Mol Sci.* 2024;25:6210. <https://doi.org/10.3390/ijms25116210>.
12. Li M, Lee K, Hsu M, Nau G, Mylonakis E, Ramratnam B. Lactobacillus-derived extracellular vesicles enhance host immune responses against vancomycin-resistant enterococci. *BMC Microbiol.* 2017;17:1–8. <https://doi.org/10.1186/s12866-017-0977-7>.
 13. Park JY, Kang CS, Seo HC, Shin JC, Kym SM, Park YS, Shin TS, Kim JG, Kim YK. Bacteria-Derived extracellular vesicles in urine as a novel biomarker for gastric cancer: integration of liquid biopsy and metagenome analysis. *Cancers.* 2021;13:4687. <https://doi.org/10.3390/cancers13184687>.
 14. Moore KA, Petersen AP, Zierden HC. Microorganism-derived extracellular vesicles: emerging contributors to female reproductive health. *Nanoscale.* 2024;16:8216. <https://doi.org/10.1039/d3nr05524h>.
 15. Luo ZW, Xia K, Liu YW, Liu JH, Rao SS, Hu XK, Chen CY, Xu R, Wang ZX, Xie H. Extracellular vesicles from *Akkermansia muciniphila* elicit antitumor immunity against prostate cancer via modulation of CD8 + T cells and macrophages. *Int J Nanomed.* 2021;2949–63. <https://doi.org/10.2147/IJN.S304515>.
 16. Grange C, Dalmaso A, Cortez JJ, Spokeviciute B, Bussolati B. Exploring the role of urinary extracellular vesicles in kidney physiology, aging, and disease progression. *Am J Physiol Cell Physiol.* 2023;325:C1439–50. <https://doi.org/10.1152/ajpcell.00349.2023>.
 17. Mizutani K, Kawakami K, Horie K, Fujita Y, Kameyama K, Kato T, Nakane K, Tsuchiya T, Yasuda M, Masunaga K, Kasuya Y, Masuda Y, Deguchi T, Koie T, Ito M. Urinary exosome as a potential biomarker for urinary tract infection. *Cell Microbiol.* 2019; 21: e13020.
 18. Tulkens J, De Wever O, Hendrix A. Analyzing bacterial extracellular vesicles in human body fluids by orthogonal biophysical separation and biochemical characterization. *Nat Protoc.* 2020;15:40–67. <https://doi.org/10.1038/s41596-019-0236-5>.
 19. Simonsen JB. What are we looking at?? Extracellular vesicles, lipoproteins, or both?? *Circ Res.* 2017;121:920–2. <https://doi.org/10.1161/CIRCRESAHA.117.311767>.
 20. Krivitsky V, Krivitsky A, Mantella V, Greenwald MBY, Sankar DS, Betschmann J, Bader J, Zoratto N, Schreier K, Feiss S, Walker D, Dengjel J, Werner S, Leroux JC. Ultrafast and controlled capturing, loading, and release of extracellular vesicles by a portable microstructured electrochemical fluidic device. *Adv Mat.* 2023;35:2212000. <https://doi.org/10.1002/adma.202212000>.
 21. Tian C, Wang K, Zhao M, Cong S, Di X, Li R. Extracellular vesicles participate in the pathogenesis of sepsis. *Front Cell Infect Microbiol.* 2022;12:1018692. <https://doi.org/10.3389/fcimb.2022.1018692>.
 22. Rodriguez-Nogales A, Algieri F, Garrido-Mesa J, Vezza T, Pilar Utrilla M, Chueca N, Garcia F, Olivares M, Rodriguez-Cabezas ME, Galvez J. Differential intestinal anti-inflammatory effects of *Lactobacillus fermentum* and *Lactobacillus salivarius* in DSS mouse colitis: impact on MicroRNAs expression and microbiota composition. *Mol Nutr Food Res.* 2017;61:1700144. <https://doi.org/10.1002/mnfr.201700144>.
 23. Naghmouchia K, Belguesmia Y, Bendali F, Spano G, Seal BS, Drider D. *Lactobacillus fermentum*: a bacterial species with potential for food preservation and biomedical applications. *Crit Rev Food Sci Nutr.* 2020;20:3387–99. <https://doi.org/10.1080/10408398.2019.1688250>.
 24. Drage LKL, Robson W, Mowbray C, Ali A, Perry JD, Walton KE, Harding C, Pickard R, Hall J, Aldridge PD. Elevated urine IL-10 concentrations associate with *Escherichia coli* persistence in older patients susceptible to recurrent urinary tract infections. *Immun Ageing.* 2019;16:1–11. <https://doi.org/10.1186/s12979-019-0156-9>.
 25. Nečas D, Klapetek P. Gwyddion: an open-source software for SPM data analysis. *Open Phys.* 2012;10:181–8. <https://doi.org/10.2478/s11534-011-0096-2>.
 26. Bader J, Rüedi P, Mantella V, Geissshüsler S, Brigger F, Qureshi BM, Ortega Arroyo J, Montanari E, Leroux JC. Loading of extracellular vesicles with nucleic acids via hybridization with Non-Lamellar liquid crystalline lipid nanoparticles. *Adv Sci.* 2025;12:2404860. <https://doi.org/10.1002/advs.202404860>.
 27. Zhou G, Wang Q, Wang Y, Wen X, Peng H, Peng R, Shi Q, Xie X, Li L. Outer membrane porins contribute to antimicrobial resistance in Gram-Negative bacteria. *Microorg.* 2023;11:1690. <https://doi.org/10.3390/microorganisms11071690>.
 28. Nie D, Hu Y, Chen Z, Li M, Hou Z, Luo X, Mao X, Xue X. Outer membrane protein A (OmpA) as a potential therapeutic target for acinetobacter baumannii infection. *J Biomed Sci.* 2020;27:1–8. <https://doi.org/10.1186/s12929-020-0617-7>.
 29. Palomino MM, Allievi MC, Gordillo TB, Bockor SS, Martin JF, Ruzal SM. Surface layer proteins in species of the family lactobacillaceae. *Microb Biotechnol.* 2023;16:1232–49. <https://doi.org/10.1111/1751-7915.14230>.
 30. Jacobson KH, Gunsolos IL, Kuech TR, Troiano JM, Melby ES, Lohse SE, Hu D, Chrisler WB, Murphy CJ, Orr G, Geiger FM, Haynes CL, Pedersen JA. Lipopolysaccharide density and structure govern the extent and distance of nanoparticle interaction with actual and model bacterial outer membranes. *Environ Sci Technol.* 2015;49:10642–50. <https://doi.org/10.1021/acs.est.5b01841>.
 31. Pradhan D, Gulati G, Avadhani R, Rashmi HM, Soumya K, Kumari A, Gupta A, Dwivedi D, Kaushik JK, Grover S. Post-biotic Lipoteichoic acid of probiotic *Lactobacillus origin* ameliorates inflammation in HT-29 cells and colitis mice. *Int J Biol Macromol.* 2023;236:123962. <https://doi.org/10.1016/j.ijbiomac.2023.123962>.
 32. Chuo STY, Chien JCY, Lai CPK. Imaging extracellular vesicles current and emerging methods. *J Biomed Sci.* 2018;25:1–10. <https://doi.org/10.1186/s12929-018-0494-5>.
 33. Harvey KL, Jarocki VM, Charles IG, Djordjevic SP. The diverse functional roles of elongation factor Tu (EF-Tu) in microbial pathogenesis. *Front Microbiol.* 2019;10:2351. <https://doi.org/10.3389/fmicb.2019.02351>.
 34. Torres AN, Veloso NC, Costa P, Cádiz L, Del Canto F, Venegas SA, Nitsche ML, Coloma-Rivero RF, Montero DA, Vida RM. Deciphering additional roles for the EF-Tu, l-Asparaginase II and ompT proteins of Shiga Toxin-Producing *Escherichia coli*. *Microorganisms.* 2020;8:1184. <https://doi.org/10.3390/microorganisms8081184>.
 35. Chung IC, Huang WC, Huang YTS, Chen ML, Tsai AW, Wu PY, Yuan TT. Unrevealed roles of extracellular enolase-1 (ENO1) in promoting Glycolysis and pro-cancer activities in multiple myeloma via hypoxia-inducible factor 1 α . *Oncol Rep.* 2023;50:205. <https://doi.org/10.3892/or.2023.8642>.
 36. Krzyzek P, Marinacci B, Vitale I, Grande R. Extracellular vesicles of probiotics: shedding light on the biological activity and future applications. *Pharmaceutics.* 2023;15: 522. <https://doi.org/10.3390/pharmaceutics15020522>.
 37. Antikainen J, Kuparinen V, Lähtenmäki K, Korhonen TK. Enolases from Gram-positive bacterial pathogens and commensal lactobacilli share functional similarity in virulence-associated traits. *FEMS Immunol Med Microbiol.* 2007;51:526–34. <https://doi.org/10.1111/j.1574-695X.2007.00330.x>.
 38. Gámez-Valero A, Lozano-Ramos SI, Bancu I, Lauzurica-Valdemoros R, Borrás FE. Urinary extracellular vesicles as source of biomarkers in kidney diseases. *Front Immunol.* 2015;6:6. <https://doi.org/10.3389/fimmu.2015.00006>.

39. Ware JP, Shea DK, Nicholas SL, Stimson EA, Riesterer JL, Ibsen SD. Recovery and analysis of bacterial membrane vesicle nanoparticles from human plasma using dielectrophoresis. *Biosensors*. 2024;14:456. <https://doi.org/10.3390/bios14100456>.
40. Ribeiro CMS, Hermsen T, Taverne-Thiele AJ, Savelkoul HFJ, Wiegertjes GF. Evolution of recognition of ligands from Gram-Positive bacteria: similarities and differences in the TLR2-Mediated response between mammalian vertebrates and teleost fish. *J Immunol*. 2010;184:2355–68. <https://doi.org/10.4049/jimmunol.0900990>.

Publisher's note Springer Nature remains neutral with regard to jurisdictional claims in published maps and institutional affiliations.